The Effect of 'Butterfly skin' with Rough Internal Surface on the Performances of an Oscillating Airfoil

Igor S. Kovalev
Science and Technology Laboratory, Kinneret College, Emek Hayarden, 15132, Israel.
Email: kovis@ashdot-m.org.il

Received date: 3/19/2014; Accepted date: 7/22/2014

ABSTRACT
An experimental investigation was conducted of the effect of 'butterfly skin' (metallic version of the butterfly scale) with rough internal surface on vibration and aerodynamic performances of a two-dimensional, 100-mm chord, NACA-230 airfoil oscillating through simulation of flare maneuver, in a 250 × 750 mm low-speed straight through a wind tunnel. Attention was initially directed to this problem by observation of the rough surfaces of butterfly wing scale as well as other studies indicating the vibration suppression of flying butterfly and the better lift of these wings by wing appendages. Results indicated that the 'butterfly skin' increased the lift force by a factor of 1.05, and reduced both the duration of vibration by a factor of 1.13, and the frequency of an oscillating airfoil by a factor of 1.5. The modification of the vibration effects on the rotor blade model was due both to an increase in the added mass, which influences the 'the butterfly skin', and to a decrease of the internal air flow velocity by aerodynamically rough surfaces of the air cavity. The total air mass which influences the slender wing with the 'butterfly skin' was represented as the sum of air mass of three geometrical figures: a circular cylinder around the wing and two right-angled parallelepipeds within the air cavity. The "butterfly skin" can have constant clear spacing of the air cavity or tapered air cavity. The interaction mechanism of a 'butterfly skin' with a flow is also described.

Key Words: added mass; 'butterfly skin'; flare maneuver; internal flow; lift; rotor blade; rough internal surface; vibration.

1. INTRODUCTION

A progressive orientation in scientific work is to apply biological methods found in living organisms in order to solve engineering problems. For example, Norberg R.A. [1] investigated the flight of dragonflies. The studies showed that the pterostigma (a pigmented spot to the leading edge of insect wing) on the one hand reduced the wing vibrations on the other hand raised the flight speed. The pterostigma of insect wing functioned like the balance weights of a helicopter rotor blade. These weights eliminated inertial dissimilarity between the blades and minimize vibration of the rotary wings [2].

1.1. Scale Coverage of *Lepidopterans* and Hollow Wing Scale

Butterflies and moths both belong to the insect order *Lepidoptera*. These insects are usually called *Lepidopterans*. The world "Lepidoptera" is derived from the Greek word meaning "scale wing". The surface of the wings of these insects is covered with millions of tiny movable appendages – scales (S_m, S_{1st} and S_{2nd} (Fig. 1)). Each scale is attached to the wing membrane *WM* by short stalk S_t, which fit into tubular socket S_o (Fig. 1b). The wing appendages and the wing are separated by scale wing clearance. The butterfly scales are arranged in highly ordered rows in the same fashion as slate tiles on a roof. In most butterflies there is one layer of these scales (Fig. 1a) or two distinct layers (Fig. 1b) on insect wings. As rule, the scale coverage of the sub marginal area (wing tip) on butterfly wings is mono-layered (Fig. 1a), and one of the basal area (wing root) of wings is multi-layered (Fig. 1b). The wing surface which is covered with two layers of scales is only 5 percent of the wing surface which

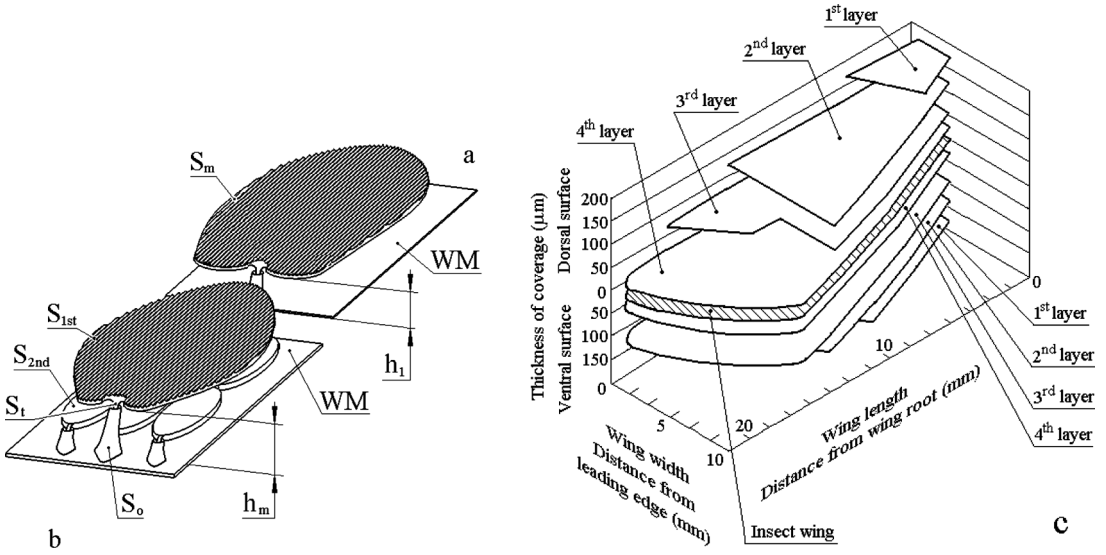

Figure 1. Scale wing clearance in different scale coverages of *Lepidopterans.* (a) Schema of mono-layered butterfly scale coverage. Magnification – 1000 times (× 1000). (b) Schema of multi-layered coverage (× 1000). (c) Structure of scale coverage on forewing of cabbage moth *Barathra Brassicae L*. [3] h_1 – hollow region of mono-layered butterfly scale coverage, h_m – hollow region of multi-layered coverage, S_m – scale of mono-layered butterfly scale coverage, S_o – socket, S_t – stalk, S_{1st} – scale of 1st layer, S_{2nd} – scale of 2nd layer, *WM* – wing membrane.

is covered with one layer of scales. So, it is generally considered that on the one hand the scale coverage of butterfly is mono layered; on the other hand the scale wing clearance is constant and invariable in gliding flight. Moreover, studies showed that the more the number of layers of butterfly scale coverage the large the magnitude of scale wing clearance is ($h_m > h_1$) (Fig. 1). The moth scale coverage is more compound than the butterfly scale coverage. For example, the thickness of the scale coverage on forewing of cabbage moth *Barathra Brassicae L.* (Fig. 1c) and the height of the scale wing clearance are decreased in direction from the basal area to the sub marginal area, and in direction from the costa (leading) edge to the trailing edge. In general, the scale wing clearance of the ventral surface (lower wing surface) of the wing is large than clear spacing of the dorsal surface (upper wing surface) (Fig. 1c) [3].

The distinction between butterfly scale coverage and moth scale coverage is due both to the different aerodynamics of the wing and to the different conditions of the flight. In nature, some butterflies use the gliding flight[4]. For straight and level flights, air flows over all areas of butterfly wings at constant airspeed and at constant glide angle. So, wing scale coverage is one or two – layered. In contrast, for most moths the flight is flapping. The moth wings rapidly change the angle of attack. Moreover, the sub marginal area of moth wings and the marginal area are traveled through the air at different angles of attack and at different airspeeds. Therefore, the wing scale coverage is multi – layered, and more complex than the butterfly scale coverage.

The microstructure of the hollow wing scale (Fig. 2a) [5] is a true miracle of nature. The scale of this tape consist of lower *LL* and upper *UL* laminae (Fig. 2b). These laminae are separated by a hollow region and are connected by trabeculae *T*. The structure of the lower lamina is undifferentiated; both surfaces of the lamina are smooth. This lamina forms a long and flattened shape of the butterfly scale. The upper lamina is a complex micro structure consisting of longitudinal ridges which are connected by cross ribs *CR*, and together they frame co-called windows to the scale interior. Overlapping lamellae *L* and micro ribs *MR* (spacing 150 nm), which are perpendicular to the lamellae and to the flow of surrounding air 1, form the longitudinal ridges. The inverted V-profile of the longitudinal ridges form the micro channels, which are disposed between the rough upper lamina and smooth lower lamina.

The scale microstructure and scale coverage of butterflies are multifunctional. Laboratory and nature examinations showed that the presence of the scales minimized the vibration of the flapping butterfly

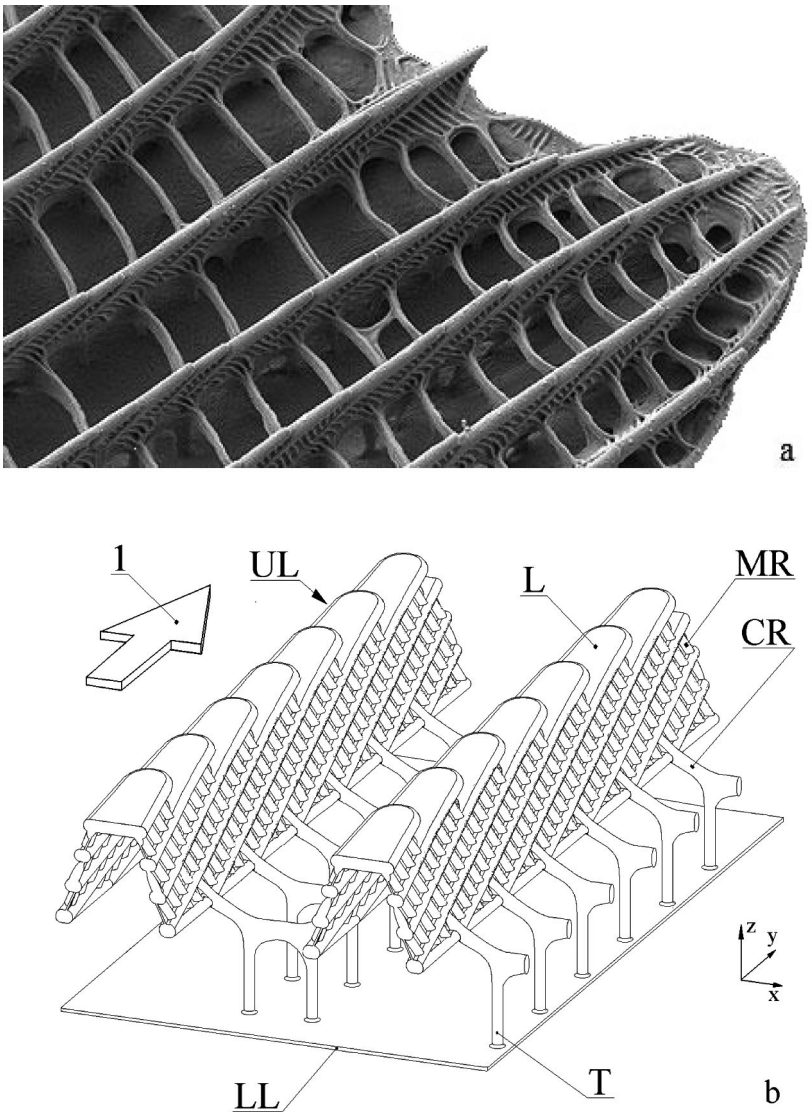

Figure 2. Fragments from hollow wing scales. (a) Electron micrograph of sub marginal area (border) of hollow wing scale on the wing of *Gonepteryxr hamni.* Side view (×100000) [5]. General structure of hollow wing scale. Vertical cross-section (×150000). *CR* – cross rib; *L* – lamella; *LL* – lower lamina, *MR* – micro rib; *T* – trabecula; *UL* – upper lamina, 1 – flow of surrounding air.

Vanessa urticae L. [6], extended the movement capability of moth *Tinea tapotialla T* [7], and increased the lift of fixed-wings of the nocturnal moth (*Catoealer*) [8]. In addition, among all present day insects, butterflies and moths with scale coverage are the record holders of two titles: long distance travel (butterfly *Danaus plexippus L.*) and flight speed (the flight speed of the moth *Agrotis ipsilo* was 113 km/h) [9]. This motivated the work presented in this paper.

In a patent application I have made suggestions to manufacture the butterfly scale [10].

1.2. Flare Maneuver of Helicopter

After loss of power due to engine failure, the helicopter has the capability of making an autorotation landing. Near the ground the pilot must flare the helicopter. The flare maneuver requires that the collective pitch angle be raised to increase the thrust and decelerate the helicopter[2]. However, rapidly increasing the angle–of–attack of airfoil generates the periodic forces (aerodynamic and inertial) at the root of the blade, which are transmitted to the helicopter airframe, producing a periodic vibratory response. Excessive vibration of rotary wing can be detrimental to the structural integrity of aircraft or

can constraint of the helicopter speed and maneuver capability. To avoid such failures, designers of aircraft incorporate various devices into wing structure in order, on the one hand, to increase the damping of rotor blade, on the other hand, to increase the lift of wing and to extend the maneuver capability of the aircraft. Applying different friction dampers is effective device in suppressing vibration of rotor blade.

The rate of descent in autorotative flight may be slow. For example, the minimum rate of autorotative descent of helicopter Mi-8 is only 5 m/s [11]. Real autorotation occurs at a higher rate of descent. Typically, the rate is between 15 m/s – 25 m/s^2.

Simulations of an angle-of-attack change of a helicopter blade in a wind tunnel have been conducted on both two-dimensional airfoil [12] and on rotor [13]. N. Ham and M. Garelick [13] tested a helicopter blade at Reynolds number of 344000; pitching rate of blade was varied between 2 and 20 radians per second [13].

1.3 'Butterfly skin'

Experimentally investigations of the wing skin, called 'butterfly skin' (metallic version of the butterfly scale) (Fig. 3a) showed that this skin, at a Reynolds number of 2×10^5 (the air speed of the wind tunnel was 30 m/s), modified the aerodynamic effects and the vibration performance on the oscillating airfoil (Fig. 3b and 3c) [14]. On the one hand, 'butterfly skin' increased the lift force by a factor of 1.15. On the other hand, the wing skin reduced the damping coefficients of oscillating blade by a factor of 1.37. The internal and external surfaces of "butterfly skin" were aerodynamically smooth [14]. Other studies [7, 29, 30] also showed that the 'butterfly skin' with aerodynamically smooth surfaces increased the duration of vibration.

However, excessive duration of airfoil vibration increases maintenance cost, passenger discomfort and pilot fatigue. Consequently, to avoid the major problem, researchers have to develop a new design of 'butterfly skin'.

Studies of insect flight mechanics have elucidated some novel and unique phenomena. Hollow wing scales of *Lepidopterans* (Fig. 2) do not exhibit the smooth section profile of scale associated with modern skin, such as a shark skin [15], "riblets" skin [16] and 'butterfly' one [14]. Their section profiles have corrugations; electron micrographs of these ridge corrugations show peak-to-peak amplitudes of 15 percent of the ridge height (Fig. 2b). This study researched the influence of the 'butterfly skin' with rough internal surface on the virtual mass and damping coefficient of an oscillating airfoil. Previous studies have not reported equivalent measurements at these aerodynamically low Reynolds numbers. There is no the intention here to tailor a particular aircraft's skin for these Reynolds number applications, but rather to illustrate trends associated with ridge corrugations that occur in nature, and then, to apply the aerodynamically rough surface into the 'butterfly skin' in order to eliminate the problems of helicopter blades.

1.4. Damping Effect and Added Mass of Surrounding Air

The result of the rapidly changing angle-of-attack of a rotary wing is damped flapping motion of a blade [2]. Vibration performances and aerodynamic forces of an oscillating airfoil are described by added mass and damped coefficients [17]. The motion of a solid blade in an air flow can be explained by a lamped

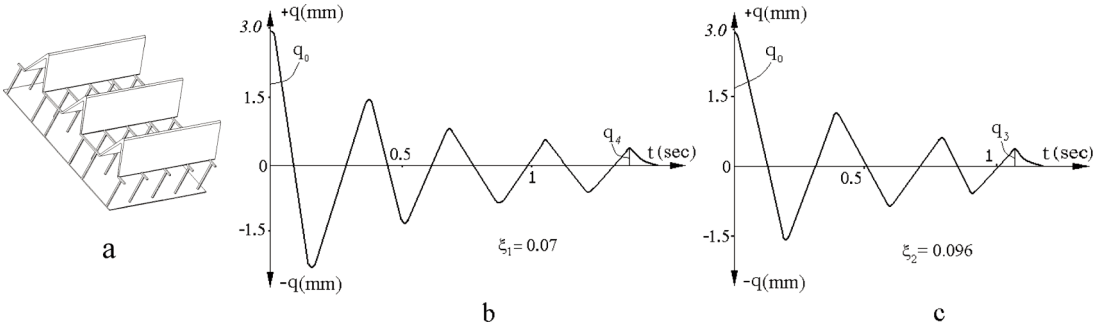

Figure 3. (a) 'Butterfly skin' [14], (b) Damped oscillating of turbine blade with 'butterfly skin', (c) Damped oscillating of turbine blade with smooth skin. q – amplitude, t – time, ξ – damping ratio.

parameter model [18] as shown in Fig. 4a. In this model m stands for total mass of flapping blade, C – total damping, k – stiffness of blade, F – force, q – motion and G – ground. The differential equation of motion for the above described model of blade can be written as [19]

$$m\ddot{q} = C\dot{q} + kq = F \tag{1}$$

m may be determined by:

$$m = m_b + m_a, \tag{2}$$

where m_b – solid blade mass; m_a – added air mass. C may be determined by:

$$C = C_b + C_a, \tag{3}$$

where C_b – damping of oscillating airfoil; C_a – added damping.

Damping is the process by which vibration steadily reduces its amplitude and duration. The rate at which the vibration amplitude decays is controlled by the damping ratio ξ. The added damping is the reduction of the vibration performance of oscillating blade by the vibration suppression devices [20].

The added mass (the virtual mass) is a portion of the surrounding air that accelerated as though it were rigidly attached to the structure [19]. In general the added mass is a function of the geometry, structure, body weight, velocity, and the vibration amplitude.

Alternatively, the rotor blade can be modeled as a simple cantilever beam (blade) [2, 21], as shown in Fig. 4b. In this scheme q stands for beam deflection and l – length of beam. The force F of the flapping elastic blade can be calculated by simple beam bending theory.

$$F = 3\ EI_x q/l^3, \tag{4}$$

where E is Young's modulus; I_x is the second moment of the cross section area.

1.5. Effect of Internal Fluid Flow

The influences of internal fluid flow on the vibration properties of structures, such as natural frequency, damping and stability, have been studied for over 60 years [22]. Experimental studies showed that, on the one hand, small flow velocity induces damping in all modes of the cantilever pipes conveying fluid, indicating that the system is stable, on the other hand, at sufficiently high flow velocity, the system becomes unstable [23].

The focus of the present paper is to simulate the angle-of-attack raise of a rotor blade model through flare maneuver and to research the influence of a 'butterfly skin' with rough internal surface on vibration and aerodynamic performances of oscillating airfoil. The experimental results are presented first.

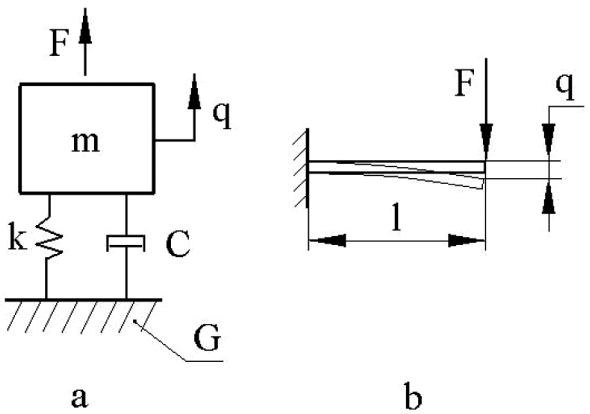

Figure 4. (a) Lumped parameter model for solid blade, (b) Scheme of the cantilever beam subjected to an end force in small deformation.

2. MATERIAL AND EXPERIMENTAL METHODS

2.1. Wind-tunnel

The aerodynamic properties of rotor blades were tested in the Zaporozhye Machine-Building Design Bureau low speed straight through wind-tunnel (Fig. 5). Air was driven from the high pressure storage *HPS* through the valve *Va* into the wide chamber *WC* (diameter of 10000 mm) where its velocity was low. The screen *S* of wire gauze helped to equalize the velocity, across the cross-section of the chamber. The honeycomb *H* ensured that there was no large-scale swirling around in the channel, but that the air traveled along it in straight lines. The irregularity of wind of the wide chamber was swamped by the large space. Thus the uniform increase in velocity that occurred when the air passed through the much narrower nozzle *N* (250 mm × 750 mm in size) was attained. The contraction section of the nozzle was designed using a matched pair of cubic curves. Thus, the wind in the working section was uniform and laminar. The air speed of the wind tunnel was 30 m/s. One typical Reynolds based on chord length on this wind speed was 200000.

Test section winds were measured using a Pitot-static tube connected to a Datametric Barocel Electronic Manometer. Pressure differences down to 0.0001 in H_2O could then be measured. Turbulent velocity data and mean speed were also measured by using a constant temperature hot-wire anemometer. The temperature of the air was maintained at 20°C.

2.2. Airfoils

Two different airfoils were used. The skin of the first airfoil was imitated from the hollow wing scale (Fig. 2b). This skin, called 'butterfly skin' was 333 times life size (the thickness was 1 mm) (Fig. 6). 'Butterfly skin' was composed of two layers. The upper metal wall *UW* and the lower metal wall *LW* were separated by an air cavity (0.4 – 0.7 mm in clear spacing). Both sides of the upper wall were covered with a large number of spanwise grooves. The depth of each groove was 0.5 mm. The ridges *Ri* (spacing 1 mm) with an inverted V-profile were formed between grooves. The grooves of the external surface were provided with lines of perforations (each opening was 0.4 mm × 0.4 mm in size).

The inverted V-profile of the ridges formed the channels, which were disposed between the upper metal wall and lower wall. The lower metal wall was similar to a thin sheet. The internal surfaces of recess were covered with a large number of micro corrugations, which were perpendicular to the ridges *Ri*, and to the flow of surrounding air 1. The depth of each corrugation was 0.05 mm.

The second airfoil was geometrically similar to the first wing (the airfoil was NACA 230; the chord of the wings was 100 mm and the length was 250 mm). It was the principal concern of this study to qualitatively determine the effect of 'butterfly skin' with rough internal surface on vibration and aerodynamic performance of an oscillating airfoil. Therefore, the skin of the second rotor blade was mono-layered, smooth and airproof. The design of the skin is traditional for modern rotor blade. These properties of the first airfoil were compared with that of the second airfoil.

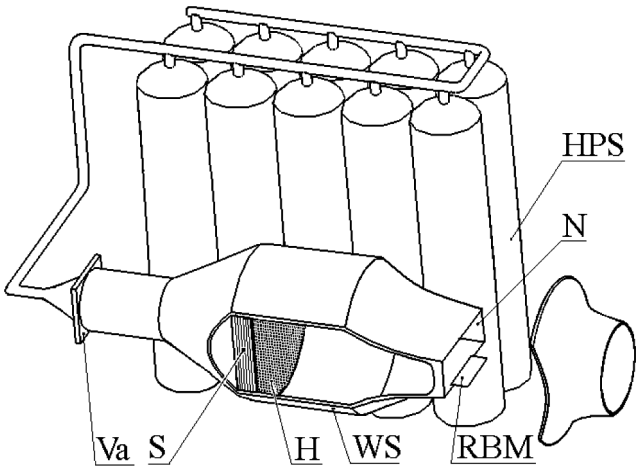

Figure 5. Scheme of the straight through wind-tunnel. *H* – honeycomb flow straightened; *HPS* – high pressure storage; *N* – nozzle; *RBM* – rotor blade model; *S* – screen; *Va* – valve; *WC* – wide chamber.

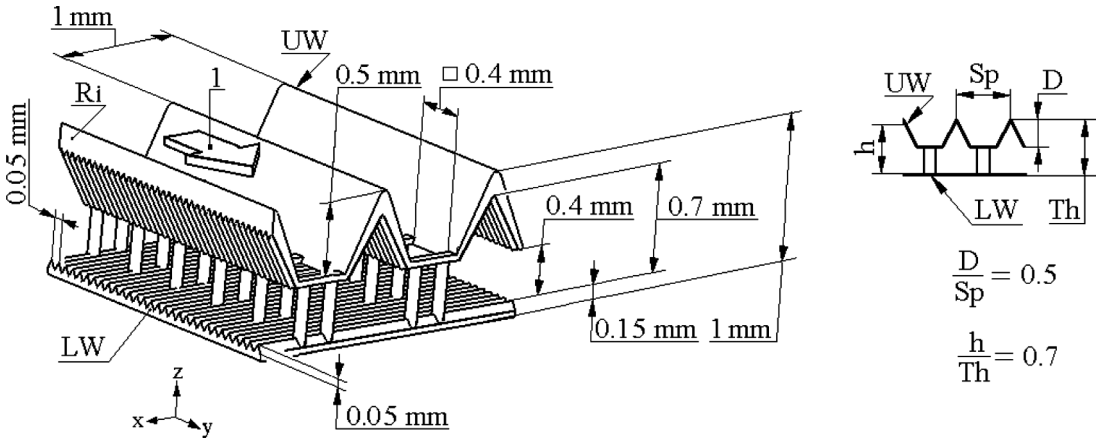

Figure 6. A vertical cross-section of the 'butterfly skin'. *LW* – lower wall; *Ri* – ridge; *UW* – upper wall; 1 – flow of surrounding air.

The special arrangement rapidly raised the angle–of–attack of the airfoils from 0 to 20 degree about their longitudinal axis in the wind tunnel. The pitching rate of the two blades was 20 degrees/sec. Two different airfoils were subjected to the same flow at identical angles of attack.

2.3. Instrumentation

The vibratory response apparatus consisted of a small piezoelectric accelerometer (model Kistler 8704B100), an oscilloscope *O* (model Hawlett-Packard), and a multichannel recorder *Re* (model Philips) (Fig. 7). The forces on the airfoils were measured using a force balance. The balance was designed for a measurement range between 0.1 mm and 10 mm amplitude of flapping motion of tip edge. The calibration accuracy and the resolution at low speeds was ± 0.1 mm amplitude. The suspension of the balance was the beam spring *BS* (Fig. 7). The width of the beam spring was 30 mm and the thickness was 5 mm. Four strain gauges *SG* (Fig. 7) (gauge type CEA-13-125 UW-120) were mounted on both sides of the beam spring. Each force sensing element was attached to the longitudinal axis of the balance suspension. Two orthogonally pairs of the transducers were wired in full bridge configuration. The sensitivity of the transducer to an excitation of 10 V was 700 NV^{-1} and 740 NV^{-1}. The load sensitivity of the balance was adjusted by an exchangeable beam spring. Each airfoil was fixed to the force balance suspension so that the transducer channel measured the forces F_z normal to the rotor blade model *RBM* (Fig. 7). These forces were then used for further processing.

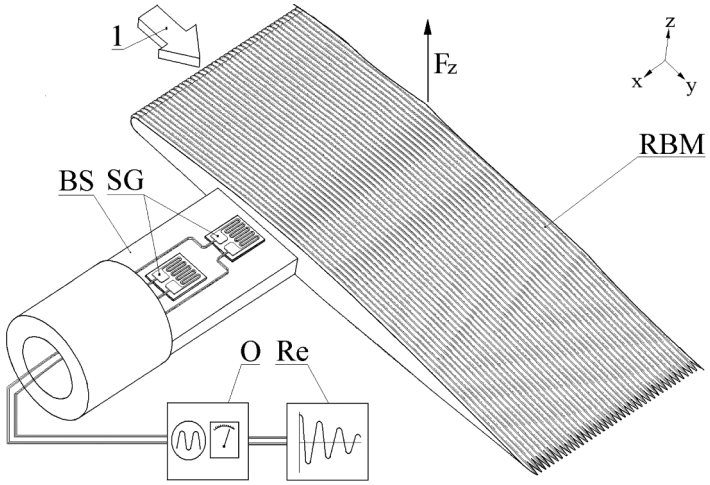

Figure 7. Fastening the strain gauges on the beam spring. *BS* – beam spring; *O* – oscilloscope; *RBM* – rotor blade model; *Re* – recorder; *SG* – strain gauges; *1* – flow of surrounding air.

3. RESULTS AND DISCUSSION

3.1. Unsteady Aerodynamic Loading

Rapidly increasing the angle–of–attack of airfoil in the flow triggered flapping motion, as was previously stated. The following sequence of unsteady environment events in both the first airfoil and the second airfoil was observed at high rates of angle–of–attack change: initially an overshoot of loading; then a decrease of the aerodynamic loading; and finally, a steady aerodynamic environment of the airfoils. As shown in Fig. 8, an aerodynamic influence on the airfoils in unsteady conditions was far more powerful than in static conditions. The character of the unsteady aerodynamic loading on the airfoil compares well with one on an airfoil for high rates of angle–of-attack change [2].

Experimental tests with metal scale models of insect wings revealed that for small deflections, corrugated beams, which were loaded as cantilevers would behave as was predicted by simple beam bending theory [24]. As shown in Fig. 7, the rotor blade models are not beams of regular cross section. It was assumed that these blades in flow would behave like cantilevered beams of regular cross section (the width of the beams was 25 mm, the thickness was 10 mm, the length was 525 mm, Young's modulus was 2.2×10^{11} Pa and the second moment of cross section area was 2.1×10^{-9} m^4), which were loaded by air force *F*.

Using the expression 4, we find that on the one hand the 'butterfly skin' with rough internal surface of the rotor blade model increases the aerodynamic loading *F* by a factor of 1.05. The increase of a lift on the airfoil with the skin was consistent with results from other studies [14]. On the other hand, aerodynamic influence on the rotor blade model with the 'butterfly skin' was less lasting than on the model with the smooth skin.

3.2. Damping Coefficients

The parameters of flapping airfoil were determined by using the Hamilton's method [25]. Amplitude of cosinusoidal oscillation of airfoil q may be described by:

$$q = q_o e^{-\xi f_n t} Cos\, f_n t \tag{5}$$

where q_0 is peak magnitude of the initial condition, ξ is the damping ratio, f_n is the undamped natural frequency, and t is time. The damping ratio ξ may be determined by:

$$\xi = \frac{\delta}{\sqrt{\delta^2 + 4\pi^2}}. \tag{6}$$

The logarithmic decrement of δ were obtained by:

$$\delta = \frac{1}{n} \ln \frac{q_o}{q_n}, \tag{7}$$

where n is the cycle number, q is the peak magnitude of this cycle. As shown in Fig. 8, the analysis of the oscillogram shows that the damping ratio of the rotor blade with the 'butterfly skin' was $\xi = 0.086$, and one of the rotor blade with the smooth skin was $\xi = 0.079$; the logarithmic decrement of the first

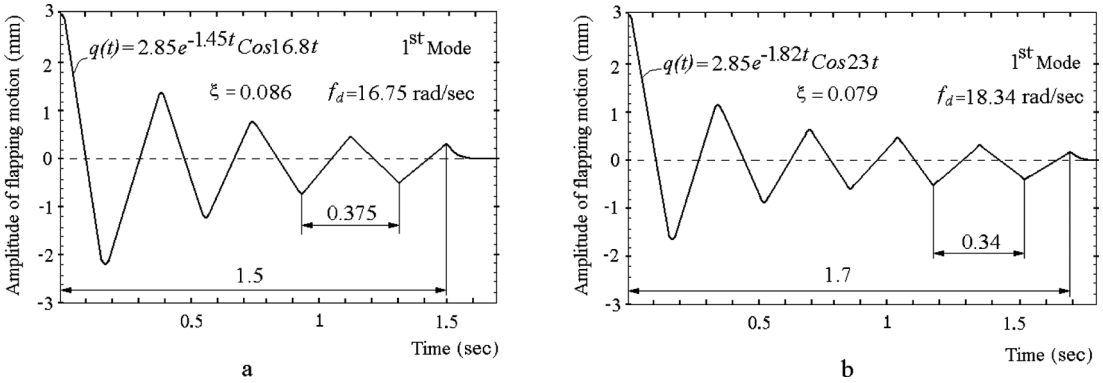

Figure 8. Damped oscillating of airfoil through simulation of flare. (a) Rotor blade model with 'butterfly skin', (b) Rotor blade model with smooth skin. f_d – damped natural frequency of rotor blade model, ξ – damping ratio.

rotor blade was δ = 0.54, and one of the second rotor blade was δ = 0.5. The calculation ξ and δ of the rotor blade with the 'butterfly skin' was based on peak magnitudes of amplitudes q_0 and q_4; the calculation ξ and δ of the rotor blade with the smooth skin was based on peak magnitudes of amplitudes q_0 and q_5 (Fig. 8). We thus see that the 'butterfly skin' with rough internal surface increases the damping ratio ξ of the flapping rotor blade model by a factor of 1.09, and as a consequence reduces the duration of vibration by a factor of 1.13.

Total damping of flapping rotor blade model *C* has two parameters (expression 3). There is damping of oscillating airfoil C_b, and there is also added damping C_a. Since in this experiment the airfoil with 'butterfly skin' and the airfoil with the smooth skin were subjected to the flow at identical damping of oscillating airfoil C_b, it follows that the increase of the total damping and of the damping ratio ξ of airfoil with the 'butterfly skin' was a result of an increase of the added damping C_a.

3.3. The Concept of the Flow and 'Butterfly skin' Interaction

Camron C. Land showed the interaction mechanism of a double wall structure of a turbine blade with a cooling fluid [26]. Wilkinson developed the interaction mechanism of a perforated wall with a turbulent viscous sub layer [27]. I developed the interaction mechanism of a 'butterfly skin' with a flow on a basis of Wilkinson's mechanism and of Land's mechanism. Fig. 9 shows a schematically drawing of what can be assumed to happen.

In Fig. 9 I plotted a local flow pattern in (Y-Z-X) plane around a cross-section of the 'butterfly skin'. The rapidly raised angle–of-attack of the rotor blade model produces a region of high pressure of air *HP* on the upper wall surface facing the mean flow *1* (Fig. 9). In this region, air is released downward perpendicularly through the holes of the perforated wall into the region of low pressure *LP* of the air cavity. The aspiration of the flow *2* in the recess produces both a pressure increase in the cavity and the air transfer *3*. The inverted V – profile of the ridges forms the miniaturized channels between the upper and lower walls. These channels as well as the ridges determine a direction of internal flow *3* (Fig. 9). Corrugations of the cavity perpendicular to the direction of air transfer 3. The region of high pressure of air *HP* on the upper wall surface forces internal flow *3* through aerodynamically rough surfaces of the air cavity. The result of the air transfer *3* in the recess with rough internal surfaces is the dissipation of energy of internal air flow *3*. As a consequence, the velocity of air travel is slowed down. Based on the work of Gregory and Païdoussis [23], it has been concluded that small velocity of internal air flow increases the damping [23] of the rotor blade model with, and reduces the duration of airfoil vibration. In other words, the damped oscillating of airfoil with 'butterfly skin' is less lasting than oscillating of airfoil with smooth skin. On the other hand, air flows faster into the recess with smooth internal surfaces [14] than into the recess with rough internal surfaces. High flow velocity of the air travel reduces the damping [23] of the structure conveying air, and increases the duration of airfoil vibration [14].

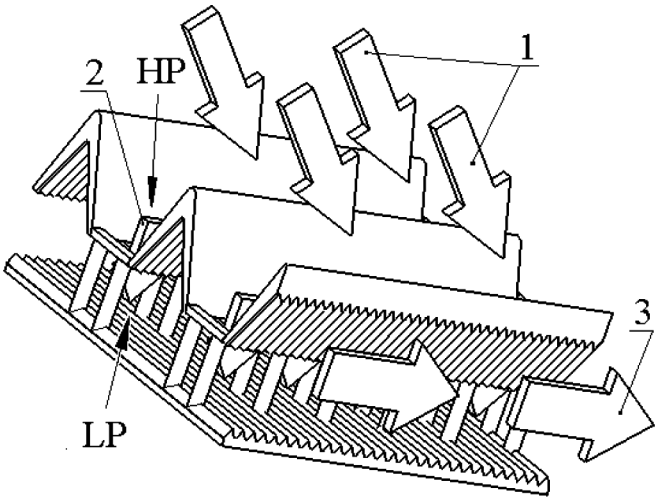

Figure 9. The influence of the flows on the surface configurations of 'butterfly skin'.
1 – mean flow; *2* – aspiration of air; *3* – internal flow, air transfer;
HP – high pressure; *LP* – low pressure.

3.4. Added Air Mass of Oscillation Airfoil

The analysis of damped oscillating of airfoil through simulation of flare (Fig. 8) shows that the 'butterfly skin' reduces the damped natural frequency f_d of the airfoil by a factor of 1.5. The natural frequency f may be approximated as follow:

$$f = \frac{1}{2\pi}\sqrt{\frac{k}{m}} \tag{8}$$

Where k is the stiffness of blade, m is the total mass of flapping of the rotor blade model (expression 2). The stiffness was 2.9×10^4 Н/м for the two models; the total mass was 1000 g for the two models. Since the airfoil with the 'butterfly skin' and the airfoil with the smooth skin were subjected to the flow at identical blade mass m_b and stiffness of blade k, it follows that the reduction of the natural frequency of the airfoil with the 'butterfly skin' f was a result of an increase of the added air mass m_a which influences the airfoil and is set in motion together with the oscillating wing. Using the expressions for the frequency f (expression 8) and the total mass m (expression 2), we find that the 'butterfly skin' increases the air mass which influences the airfoil by a factor of 1.2.

A comparison of the interaction mechanisms of the two wings shows that the rotor blade with the 'butterfly skin' interacts with mean flow *1*, enter flow *2*, and internal flow *3* (Fig. 9). On the other hand the smooth and airproof skin interacts only with mean flow. We thus see that the structure of 'butterfly skin' increases the volume of the added air which influences the skin and is set in motion together with the oscillation blade.

3.5. Air Mass Which Influences the Slender Wing

Inviscid flow theory shows that the virtual mass of a slender wing accelerated normal to its chord is equal to the mass of air in an imaginary circular cylinder around the wing with the chord as its diameter (Fig. 10a) [28]. A wing section with smooth skin thus has a virtual air mass of circular cylinder m_a' per unit span equal to

$$m_a^{'} = \frac{\pi\rho c_h^2}{4}, \tag{9}$$

where c_h is uniform-chord wing (c_h = constant), and ρ is the mass density of air. The virtual mass of the slender wing with smooth skin is given by

$$m_a = \int_0^R m_a^{'}\, dr = \int_0^R \frac{\pi\rho c_h^2}{4} dr. \tag{10}$$

Where R is the length of the wing. The total air mass which influences the slender wing with 'butterfly skin' may be represented as the sum of air mass of geometrical figures: a circular cylinder (imaginary figure), and two right – angled parallelepipeds (reality figures) (Fig. 10b). The wing section thus has an air mass m_t' per unit span equal to

$$m_t^{'} = m_a^{'} + 2m_p^{'} = \frac{\pi\rho c_h^2}{4} + 2h\rho c_h, \tag{11}$$

where m_p' – virtual mass of right – angled parallelepiped per unit span, h – clear spacing of the air cavity (h = constant).

The total air mass which influences the slender wing with 'butterfly skin' then is

$$m_t = \int_0^R m_t^{'}\, dr = \int_0^R \left(\frac{\pi\rho c_h^2}{4} + 2h\rho c_h \right) dr = \int_0^R \frac{\pi\rho c_h^2}{4} dr + \int_0^R 2h\rho c_h\, dr. \tag{12}$$

Expression 12 shows that the increase of the total air mass can be obtained, within limits, by increasing the clear layer spacing, but this increases the structural weight of the rotor blade. h_{fbr} – forward clear spacing on bottom of blade root, h_{fbt} – forward clear spacing on bottom of blade tip, h_{ftr} – forward clear spacing on top of blade root, h_{ftt} – forward clear spacing on top of blade tip, h_{rbr} – rear clear spacing on bottom of blade root, h_{rbt} – rear clear spacing on bottom of blade tip, h_{rtr} – rear clear spacing on top of blade root, h_{rtt} – rear clear spacing on top of blade tip.

By analogy with the scale coverage of *Lepidopterans,* the structure of the 'butterfly skin' can be classified as two types: one with constant clear spacing of the air cavity (Fig. 11a) and the other with variable clear spacing (Fig. 11a and 11b). The first type of skin is imitated from the butterfly scale

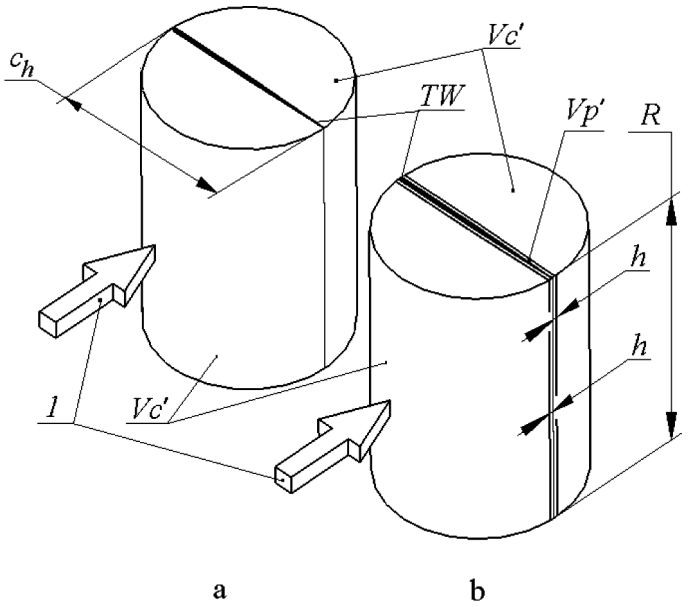

Figure 10. Air masses of different airfoils. (a) A slender wing with smooth skin, (b) A slender wing with 'butterfly skin'. c_h – airfoil chord, R – airfoil length, m_a – added air mass of circular cylinder, m_p – added air mass of right – angled parallelepiped, h – clear spacing of the air cavity, *TW* – slender wing, *1* – flow of surrounding air.

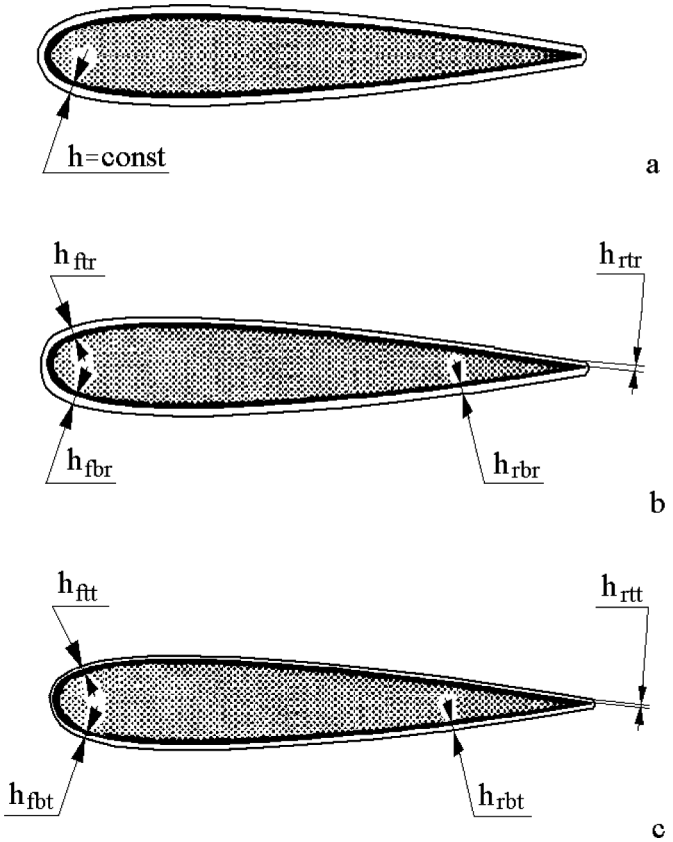

Figure 11. Different air cavities of 'butterfly skin' on parallel plan form blade (a) Rotor blade with constant clear spacing of air cavity, (b) Blade root with variable air cavity of 'butterfly skin', (c) Blade tip with variable air cavity of 'butterfly skin'.

coverage (Fig. 1a). This skin is attached to the wing surface of the aircraft which operates at constant airspeed and constant angle of attack (for example: wing of a glider). The second type of skin is imitated from the moth scale coverage (Fig. 1c). This skin is attached to the surface of the helicopter rotor blade which operates at different airspeeds and at different angles-of-attack. The height of the air cavity is decreased in direction from the blade root to the blade tip ($h_{ftr} > h_{ftt}$, $h_{rtr} > h_{rtt}$, $h_{fbr} > h_{fbt}$, $h_{rbr} > h_{rbt}$), and in direction from the leading edge to the trailing edge ($h_{ftr} > h_{rtr,}$ $h_{ftt} > h_{rtt}$, $h_{fbr} > h_{rbr}$, $h_{fbt} > h_{rbt}$); the clear spacing of the scale coverage which is attached to the lower blade surface more than one of the upper blade surface ($h_{fbr} > h_{ftr}$, $h_{rbr} > h_{rtr}$, $h_{fbr} > h_{ftt}$, $h_{rbt} > h_{rtt}$).

4. CONCLUSIONS

It thus seems that the oscillating airfoil with the 'butterfly skin' has, at a Reynolds number of 330000, the obvious advantages of lift force and reduction both of vibration duration, and frequency of an oscillation airfoil by comparison with a traditional rotor blade. The modification of the vibration effects on the model is due to an increase in the virtual air mass, which influences the 'butterfly skin' and to a decrease of the internal air flow velocity. The 'butterfly skin' can have constant clear spacing of the air cavity or tapered air cavity. The interaction mechanism of a 'butterfly skin' with a flow is also described. The total air mass which influences the slender wing with the 'butterfly skin' is represented as the sum of air mass of three geometrical figures: a circular cylinder around the wing and two right-angled parallelepipeds within the air cavity. Analytical study shows that increasing the clear spacing of the air cavity would tend to increase the total air mass even more. However, a parametric study of an air cavity was not within the scope of this experiment. A full explanation must await more detailed studies. But it does not seem unreasonable to suggest the possibility of some optimal cavity geometry and rough internal surface to further augment the lift force and to reduce the vibration of airfoil.

ACKNOWLEDGEMENTS

I would like to thank my advisor Dr. Olga Bocharova–Messner for her ideas and comments. Her input has contributed significantly to this work. I thank external reviewers for their constructive comments. The author would like to acknowledge the Zaporozhye Machine-Building Design Bureau for its collaboration. I would also like to acknowledge Mrs. Judi Rimmer for her help.

List of symbols

Roman symbols

BS	beam spring
C	total damping
C_a	added damping
C_b	damping of oscillating airfoil
CR	cross rib
c_h	airfoil chord
D	depth of groove
E	Yong's modulus
F	lift force
F_z	force, which normal to the rotor blade model
f	natural frequency of rotor blade model
f_d	damped natural frequency of rotor blade model
f_n	undamped natural frequency of rotor blade model
G	ground
H	honeycomb flow straightened
HP	high pressure
HPS	high pressure storage
h	clear spacing of the air cavity
h_m	hollow region of multi-layered coverage
h_{fbr}	forward clear spacing on bottom of blade root
h_{fbt}	forward clear spacing on bottom of blade tip
h_{ftr}	forward clear spacing on top of blade root

h_{ftt} forward clear spacing on top of blade tip
h_{rbr} rear clear spacing on bottom of blade root
h_{rbt} rear clear spacing on bottom of blade tip
h_{rtr} rear clear spacing on top of blade root
h_{rtt} rear clear spacing on top of blade tip
h_1 hollow region of mono-layered butterfly scale coverage
I_x second moment of cross section area
k stiffness of blade
L lamella
LL lower lamina
LP low pressure
LW lower wall
l length of beam
MR micro rib
m total mass of flapping rotor blade model
m_a added air mass/added air mass of circular cylinder
m_b oscillating blade mass
m_p added air mass of right – angled parallelepiped
m_t total air mass of slender wing with 'butterfly skin'
m_a' virtual mass of circular cylinder per unit span
m_p' virtual mass of right – angled parallelepiped per unit span
m_t' total air mass of slender wing with 'butterfly skin' per unit span
N nozzle
O oscilloscope
R airfoil length
RBM rotor blade model
Re recorder
Ri ridges
q amplitude of flapping motion of tip edge/motion
q_0 peak magnitude of the initial condition
S screen
SG strain gauges
S_m of mono-layered butterfly scale coverage scale
S_o socket
Sp spacing
S_t stalk
S_{1st} scale of 1st layer
S_{2nd} scale of 2nd layer
T trabecula
Th thickness of 'butterfly skin'
TW slender wing
t time
UL upper lamina
UW upper wall
Va valve
WC wide chamber
WM wing membrane

Greek symbols

ξ damping ratio
δ logarithmic decrement

Indiannumber symbols

1 mean flow/flow of surrounding air
2 aspiration of air/enter flow
3 internal flow/air transfer.

REFERENCES

[1] Norberg, R.Å., "The pterostigma of insect wings an inertial regulator of wing pitch," *Journal of Comparative Physiology A: Neuroethology, Sensory, Neural, and Behavioral Physiology*, Vol. 81, No. 1, 1972, pp. 9–22.

[2] Johnson W., *Helicopter Theory,* Princeton University Press, 1980.

[3] Kovalev, I.S., and Brodsky, A.K., "Structure and some functional characteristics of the scale coverage in the cabbage moth *Barathra brassicae L. Lepidoptera, Noctuidae*," *Entomological Review*, Vol. 75, No. 3, 1996, pp. 530–540.

[4] Dudley, R., *The biomechanics of insect flight. Form, function, evolution*, N.J., Princeton University press, 2000.

[5] Бочарова-Месснер О.М., Соколов В.Е., Евгеньева Т.П., and Наумова Е.И. Адаптивные свойства эпителия и его производных. Атлас микрофотографий, полученных при помощи электронного сканирующего микроскопа. М. Наука, 1979 г. 180 с.

[6] Kovalev, I.S., and Brodsky, A.K., "Of the role that elasticity and scale overages of the wings play in the flight stability of insects," *Bulletin of the S. Petersburg State University*, series 3, issue 3, 1996, pp. 3–7.

[7] Kovalev, I.S., "The Functional Role of the Hollow Region of the Butterfly *Pyrameisa talanta (L.)* Scale", *Journal of Bionic Engineering*, Vol. 5, No. 3, 2008, pp. 224–230.

[8] Nachtigall, W., "Die aerodinamische Funrtion der Schmetterlingsschuppen," *Naturwissenschaften*, Vol. 52, No. 9, 1965, pp. 216–217.

[9] Sappington, T.W., and Showers, W.B., "Reproductive maturity, mating status, and long-duration flight behaviour of *Agrotisipsilon* (Lepidoptera: Noctuidae) and the conceptual misuse of the oogenesis-flight syndrome by entomologists," *Environmental Entomology*, 21, 1992, pp. 677–688.

[10] Kovalev, I.S., "Aerodynamic skin," Patent application, No. 2061915, 1996.

[11] Volodko, A.M., *Fundamental principles of aerodynamics and helicopter flightd ynamics*, M. Transport, 1988.

[12] Parker, A.G., "Force and Pressure Measurements on an Airfoil Oscillating through Stall," *Journal of Aircraft*, Vol. 13, 1976, pp. 823–827.

[13] Ham, N.D., and Garelick, M., "Dynamic Stall Considerations in Helicopter Rotors," *Journal of the American Helicopter Society*, Apr. 13, 1968, p. 49.

[14] Kovalev, I.S., "From Butterfly to Wind Turbine," *Wind engineering*, Vol. 34, No. 4, 2010, pp. 351–360.

[15] Bechert, D.W., Hoppe, G. and Reif, W. E., "On the drag reduction of the shark skin," *AIAA Shear Flow Control Conf. Proc*., 12–14 Mar., 1985, p. 18.

[16] Zuniga, F.A., Anderson, B.T., and Bertelrud, A., "Flight Test Results of Riblets at Supersonic Speeds," *NASA Technical Memorandum*, 4387, 1992, p. 37.

[17] Ursell, F., "On the virtual-mass and damping coefficients for long water of finite depth," *Journalof Fluids Engineering,* Vol. 76, 1975. pp. 17–28.

[18] Ciğeroğlu1, E., and Özgüven, H.N., "Nonlinear Vibration Analysis of Bladed Disks with Dry Friction Dampers," *Journal of Soundand Vibration*, Vol. 295, 2006, pp. 1028–1043

[19] Rodriguez, C.G., Egusquiza, E., Escaler, X., Liang, Q.W., and Avellan, F., "Experimental investigation of added mass effects on a Francis turbine runner in still water," *Journal of Fluids and Structures*, Vol. 22, No. 5, 2006, pp. 699–712.

[20] Gordon, R.W., and Hollkamp, J.J., "An Internal Damping Treatment for Gas Turbine Blades," *38thAIAA/ASME/ASCE/AHS/ASC Structures*, Structural Dynamics, and Materials Conference and Exhibit and AIAA/ASME/AHS Adaptive Structures Forum, 7–11 April 1997, pp. 442–451.

[21] Peters, D.A., and Ormiston, R.A., "Flapping Response Characteristics of Hingeless Rotor Blades by a Generalized Harmonic Balance Method," *NASA*, TN D -7856, Feb. 1975.

[22] Rinaldi, S., Prabhakar, S., Vengallator, S., and Païdoussis, M.P., "Dynamics of microscale pipes containing internal fluid flow: damping, frequency shift, and stability," *Journal of Sound and Vibration*, No. 329, 2010, pp. 1081–1088.

[23] Gregory, R.W., and Païdoussis, M.P., "Unstable oscillation of tubular cantilevers conveying fluids," I. Theory. Proceedings of the Royal Society, London, 1966, pp. 512–527.

[24] Rees, C., "Form and function in corrugated insect wings", *Nature*, Vol. 256, 1975, pp. 200–203.

[25] Hamilton, J.M., "Vibration-based technique for measuring the elastic properties of ropes and the added mass of submerged objects." *Journal of Atmospheric and Oceanic Technology*, Vol. 17, No. 5, 2000, pp. 688–697.

[26] Camron, C., Chris, J., and Karen, A.T., "Considerations of a Double-Wall Cooling Design to Reduce Sand Blockage," *Journal of Turbomachinery*, Vol. 132, 2010, pp. 031011-1–8.

[27] Wilkinson, S.P., "Influence of wall permeability on turbulent boundary – layer properties," *American Institute of Aeronautics and Astronautics*, Paper No. 83 – 0294, 1983.

[28] Ellington, C.P., "The aerodynamics of hovering insect flight. II. Morphological parameters," Phil. Trans. R. Soc. Lond., B 305, 1984, pp. 23–27.

[29] Nachtigall, W. and Wisser, A., *Bionikin Beispielen*, Springer-Spektrum, 2013.

[30] Kovalev, I., "Butterflies and helicopters," *Bulletinof the Entomological Societyof Canada*, Vol. 37 (3), 2005, pp. 140–142.